ADVANCED MATERIALS
www.advmat.de

Charged Metal Nanoparticles for Chemoelectronic Circuits

Xing Zhao, Jiahui Guo, Tao Xiao, Yuchun Zhang, Yong Yan, and Bartosz A. Grzybowski**

Although metal nanoparticles (NPs) stabilized with self-assembled monolayers (SAMs) of various organic ligands have proven useful in applications ranging from chemical sensing, to bionanotechnology, to plasmonics and energy conversion, they have not been widely considered as suitable building blocks of electronic circuitry, largely because metals screen electric fields and prevent electrically tunable conductivity. However, when metal nanoparticles a few nanometers in size are stabilized by charged ligands and placed under bias, the counterions surrounding the NPs can redistribute and establish local electric fields that feed back into the electronic currents passing through the nanoparticles' metallic cores. Herein, the manner in which the interplay between counterion gradients and electron flows can be controlled by using different types of SAMs is discussed. This can give rise to a new class of nanoparticle-based "chemoelectronic" logic circuits capable of sensing, processing, and ultimately reporting various chemical signals.

1. Introduction

Electrically tunable conductivity is one of the key characteristics of materials traditionally used in electronic circuits—predominantly silicon-based semiconductors,[1] but also quantum dots,[2] organic π-conjugates,[3] and some carbon materials,[4] from which various diodes, transistors, memories, optical devices, and integrated circuits can be made. Metals do not feature on this list and serve only auxiliary roles (e.g., as wiring elements) because they screen electric fields at extremely short distances (<1 nm).[5] With the rise of nanotechnology, however, engineering of very small metallic "parts" (nanoparticles (NPs), nanorods, etc.[6]) has become possible and much effort has been devoted to the study of electronic properties of materials comprised of such elements. Many groups have demonstrated changes in conductance upon mechanical,[7] optical,[8] thermal,[9] or chemical[10] stimuli but demonstrations of electrically tunable conductivity have been far and between. Of note, the so-called single electron transistors based on metal nanoparticles have been shown to exhibit conductance varying with the applied bias—unfortunately, such devices display periodic conductance oscillations due to the well-known Coulomb-blockade effect, with the current ratios depending on the dielectric environment and/or Coulomb energy barrier between adjacent nanoparticle cores.[11] With such inherent instabilities, the notion of metal-based electronics becoming practical might not seem promising, at least for the electrical modulation of the material's electronic conductivity. We first revisited this issue around a decade ago, while working on nanoparticles covered with charged organic ligands.[12] We reasoned that if another form of mobile charge carriers—namely, the counterions surrounding the charged NPs—were present, the applied electric fields could cause their redistribution and establish internal electric fields that would then feed-back and control the motions of electrons between particle's metallic cores. In other words, we wished to achieve tunable electronic conductivity by establishing counterion gradients within a nanostructured material. Herein, we illustrate how this basic idea has since been applied to systems of increasing complexities—first, to make "polarizable" films[13] of one-type of charged NPs, then bilayer structures comprising particles of opposite polarities and serving as diodes,[14] then various types of chemical sensors,[14,15] and finally entire logic circuits in which metallic NPs serve as sensing and well as information-processing units.[14] We have called such circuits "chemoelectronic" to emphasize the ease with which metallic NPs can be chemically modified with organic ligands responsible for processing electronic signals and/or those responsible for chemical sensing. Chemoelectronic devices are easily processable (simply cast from methanolic solutions), mechanically flexible, and can selectively transduce part-per-trillion chemical changes into electrical signals, and consume relatively little power (≈μW). On the downside, they are not nearly as fast as silicon-based devices, though their speeds are commensurate with common polymer electronics.[16] We narrate these and other pros and cons toward the end of the paper where we also try to highlight the most interesting prospects (and challenges) for future studies on and applications of these unusual nanomaterials.

X. Zhao, J. Guo, T. Xiao, Dr. Y. Zhang, Prof. Y. Yan
CAS Key Laboratory of Nanosystem and Hierarchical Fabrication
CAS Center for Excellence in Nanoscience
National Center for Nanoscience and Technology
Beijing 100190, China
E-mail: yany@nanoctr.cn
J. Guo, T. Xiao, Prof. Y. Yan
University of Chinese Academy of Sciences
Beijing 100049, China
Prof. B. A. Grzybowski
IBS Center for Soft and Living Matter and Department of Chemistry
UNIST
50, UNIST-gil, Eonyang-eup, Ulju-gun, Ulsan 44919, South Korea
E-mail: grzybor72@unist.ac.kr, nanogrzybowski@gmail.com
The ORCID identification number(s) for the author(s) of this article can be found under https://doi.org/10.1002/adma.201804864.

DOI: 10.1002/adma.201804864

2. Dynamic Ionic Gradients and Current Steering

As a prototypical system exhibiting tunable conductivity we used films of ≈5 nm gold nanoparticles,[17] AuNPs, stabilized with positively charged *N,N,N*-trimethyl-(11-mercaptoundecyl) ammonium chloride ($C_{11}NMe_3^+Cl^-$, TMA) ligands. Importantly, the larger AuTMA particles in such films are jammed—like grains of sand—but the smaller Cl^- counterions can still migrate through the spaces between these particles. When the film is placed under bias (**Figure 1**a), the current initially decreases but ultimately reaches a steady-state value (Figure 1b) which depends nonlinearly on the applied bias. Since no similar effects are observed in films of NP covered with neutral ligands (they behave as simple Ohmic conductors), and because there are no Faradaic reactions at the electrodes flanking the film, the effect can be attributed to the formation of a gradient of counterions (migrating towards the "+" electrode), in turn giving rise to an internal electric field, E_i, that opposes the applied field, E_{app}, and hinders the flow of electrons through the metal cores (cf. Figure 1a; for theoretical details describing all these processes, see models in ref. [13]). The existence of such a gradient and its time evolution has been confirmed experimentally (via Kelvin probe force microscopy (KPFM) and energy-dispersive X-ray spectroscopy (EDS)[18]) and is the key feature of all the systems we discuss below. Naturally, the gradient is transient and disappears when the bias is removed, though this equilibration is a rather slow process occurring on the timescale of hundreds to thousands of seconds. As long as the

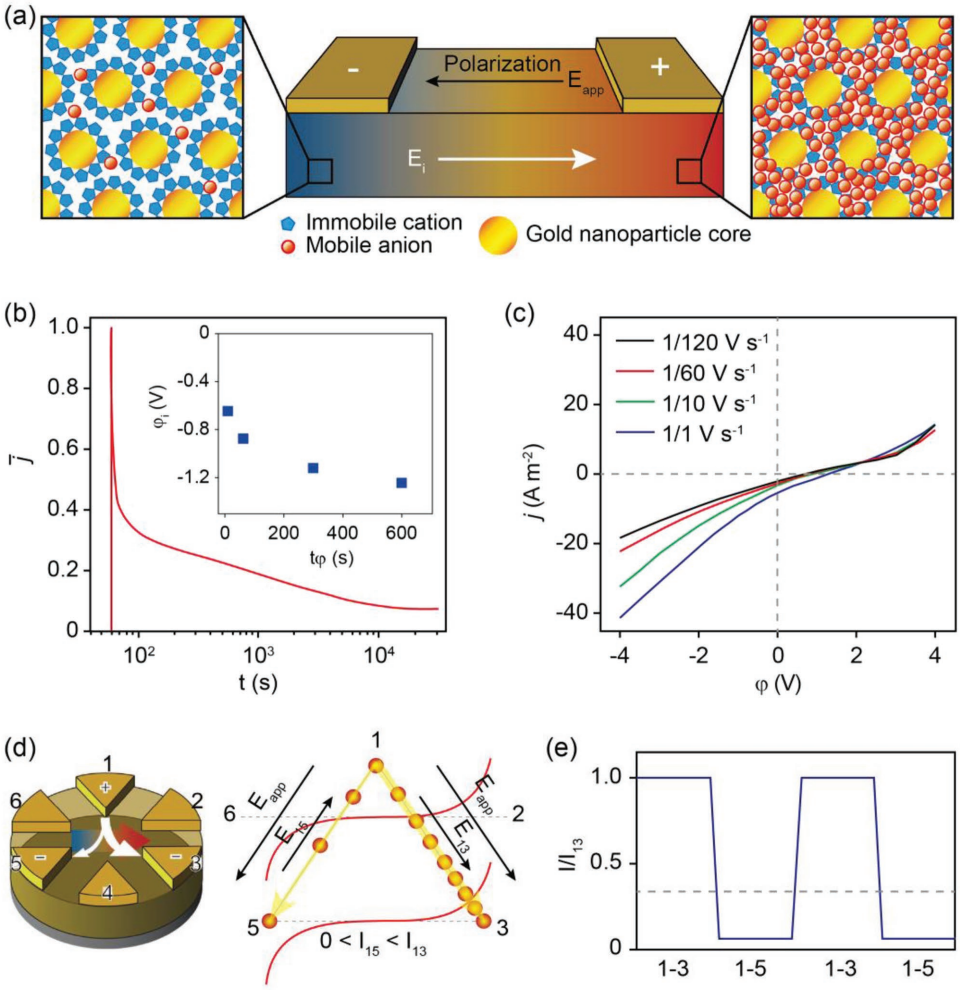

Figure 1. Dynamic ionic gradients and reconfigurable electronic components. a) Mobile counterions around immobile/jammed charged NPs (positively charged TMA AuNPs) migrate under bias and set up counterion gradients within the material. An internal electric field, E_i, is generated in the direction opposite to that of the polarization field, E_{app}. b) Normalized current density though the charged-NP film as a function of time. The inset is the internal electric potential measured in an open-circuit configuration at different polarization times (polarization potential: 4 V). c) Current–voltage, j–φ, characteristics of a TMA AuNPs film collected after initially polarizing this film at 4 V for 10 min. With the decrease of sweep rate, the curves flattens and the rectification ratio decreases. Notice that zero current does not correspond to zero voltage—instead the material ceases to conduct electrons at a nonzero applied bias. d) Current steering in a device with six wedge-shaped electrodes. Polarization potential was applied between electrodes (5,6) and (2,3). The direction of polarization is indicated by the thick, gradient arrow. Red lines give qualitative distribution of mobile anions (individual anions are represented by red spheres). e) Normalized currents along the (1–3) and (1–5) directions. e) The relative current ratio can be as high as 120, whereby the (1–5) "channel" becomes almost non-conductive and the current is effectively "deflected" towards channel (1–3). The dashed line is the relative current for both channels in the absence of polarization. Reproduced with permission.[13] Copyright 2011, Springer Nature.

gradient persists and material is polarized, it exhibits several unique characteristics. For instance, for an initially "polarized" material there exists a nonzero voltage at which E_{app} balances E_i and the material effectively transitions from a conductor to an insulator (Figure 1c). When the direction of bias is reversed, the conductance "along the gradient" (i.e., when E_{app} and E_i point in the same direction) is higher (up to hundred times) than in the opposite direction—in other words, the polarized NP film can rectify electronic currents. Finally, when the counterion gradients are first established in one direction and then currents are passed in another direction, these gradients can prevent the current from flowing through some parts of the material and effectively be "steered" toward other regions—in Figure 1d,e, polarizing bias applied between electrodes (5,6) and (2,3) directs the currents from electrode 1 to either (3) or (5). Such examples serve to illustrate that films of charged NPs are, indeed, quite peculiar in their ability to polarize yet still transmit electronic currents—in contrast, conventional dielectrics can polarize but are not conductive whereas metals are conductive but cannot sustain internal electric fields countering external bias.

3. Bilayer NP Diodes

The ability to rectify current is one of the key characteristics of diodes but for the AuTMA NP films described above, the times to establish counterion gradients and to build internal fields are too long to be useful. Therefore, as an alternative, we considered systems comprised of two layers, each ≈500 nm thick, of oppositely charged NPs: positively charged TMA AuNPs surrounded by negative Cl^- counterions and negatively charged AuNPs covered with deprotonated 11-mercaptoundecanoic acid (MUA) and surrounded by $N(CH_3)_4^+$ counterions (**Figure 2**a).[14,18,19] When these two layers are in contact, entropy-driven intermixing of mobile counterions takes place—some of the Cl^- anions enter the MUA NP layers and, vice versa, some of the $N(CH_3)_4^+$ cations enter the TMA NP layer (Figure 2b). Counterions' interdiffusion continues until the entropic driving force is offset by the electric fields established across the interface—at equilibrium, this internal field can be as high as 600 V m^{-1} and exists in the absence of any bias (Figure 2c). Importantly, under bias, when negative potential is applied to the AuTMA layer, the counterions of each polarity

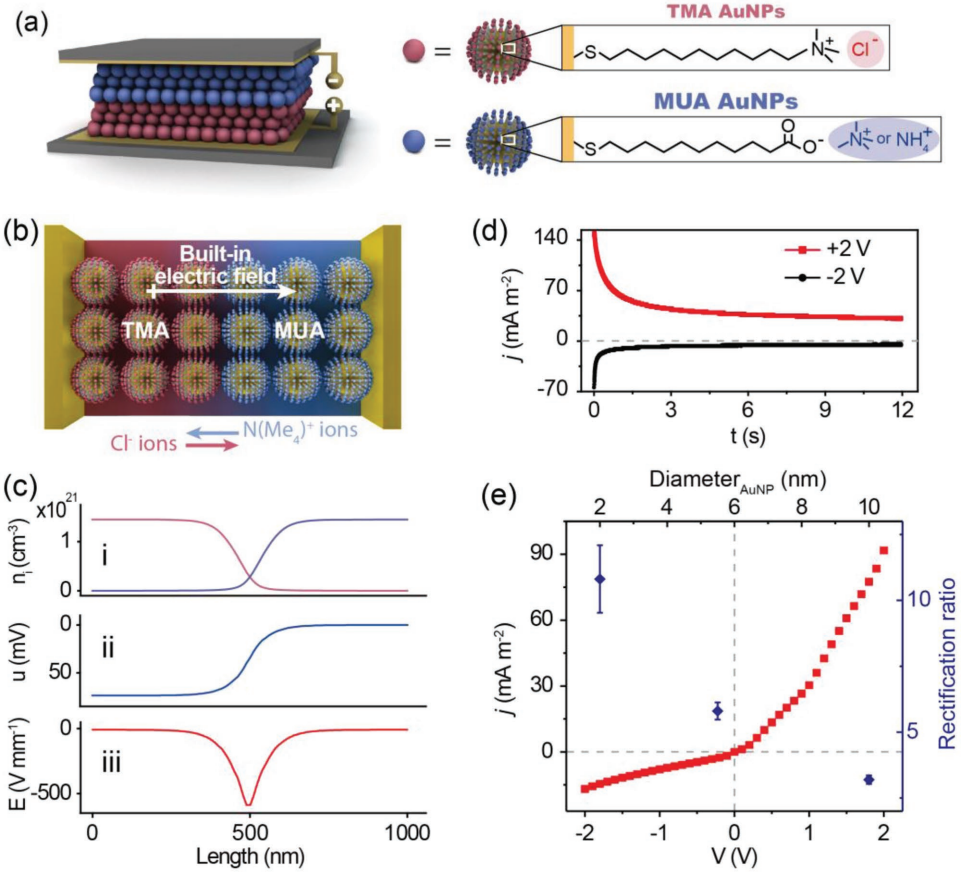

Figure 2. Bilayer metal nanoparticle diodes. a) The scheme of a metal nanoparticle diode fabricated by laminating two layers of TMA and MUA AuNPs. b) As the two layers are brought into contact, mobile counter ions interdiffuse across the interface and establish an internal electric field. c) Calculated distributions of tetramethyl ammonium cations (red) and chloride anions (blue) after equilibration (i). The corresponding potential within the device (ii). Electric field is as high as 600 V mm^{-1} at the interface (iii). Note: The ion concentration is estimated by considering the metal NP core size, surface coverage of thiols, and approximately hexagonal arrangement of AuNPs in the film (see Figure S2c in ref. [14]). d) Currents monitored for 200 s (the first 12 s are shown) after stepping the potential from 0 to +2 or −2 V. e) Current–voltage characteristics (red markers and bottom and left axes) and variation of rectification ratio with AuNP diameter (blue markers, top and right axes). Reproduced with permission.[14] Copyright 2016, Springer Nature.

are "pushed" closer to the interface and towards each other—in this way, the internal field opposing electron flow is increased and the electronic conductivity of the material is low (Figure 2d, black curve). When the bias is reversed, the counterions are pulled away from the interface, the internal field is diminished, and the conductivity is higher (Figure 2d, red curve). On the microscopic level, the concentrations of electrons in the NPs' cores remain nearly unchanged and the rectification behavior can be ascribed to the internal field modulating the heights of the barriers the electrons experience when tunneling between proximal NP metal cores (the probability of electron tunneling is increased in the direction from the MUA to the TMA layers and decreased in the opposite direction). With the mathematical models describing these phenomena detailed in refs. [13,14], we note that because the layers are very thin, the times to establish the ionic gradients are significantly shorter than the previously described current "steering" devices and the diode can be switched on timescales of tens to hundreds of milliseconds achieving rectification ratios $r \approx 4$. As could be expected, increasing thickness of the NP layers decreases the rectification ratios (from 7 at 170 nm to 4 at 1330 nm) while increasing switching times (correspondingly, from 40 to 290 ms). The rectification ratio can be boosted by increasing the concentration of counterions setting up the internal field. In particular, when NPs having smaller cores but same ligands are used, there are more counterions per unit volume and the rectification ratios increase (e.g., from $r = 3$ for 10 nm NPs to $r = 11$ for 2 nm NPs, Figure 2e, blue markers). Another approach to increase per volume counterion concentrations could be to use ligands presenting multiple charged groups or shorter thiols. In the latter case, shorter ligands would also render the edge-to-edge spacing between metal cores smaller, thus facilitating interparticle electron transport;[20] it should be remembered, though, that thinner monolayers are less stable under bias.[21]

4. Sensing Elements

Since the passage of electrons between metal cores of proximal NPs is very sensitive to the tunneling barriers due to the on-particle SAMs, small changes in the SAM induced by external "stimuli" can be effectively amplified into easily detectable electrical signals. This so-called chemoresistance has provided basis for various types of sensors for solution-based analytes[22] (down to fM, see ref. [22a]) or volatile substances (at the ppm levels[23]). Over the years, we have used and extended this principle to construct various types of sensing elements—including those based on unusual physical phenomena, such as polaron trapping[15b] or involvement of both HOMO and LUMO orbitals in electron transport[15a]—and ultimately integrated some of them into chemoelectronic circuits.

Historically, our first examples focused on photosensors in which the film's conductivity changed upon light irradiation.[15b] In particular, when the Au or Ag NPs were stabilized by charged ligands, their end-groups formed polaron-like sites capturing the electrons and reducing the current through the NP films ("negative photoconductance," see ref. [15b]). The idea of modulating currents by the charged species captured in between the NPs was then expended to ultrasensitive chemical detection. **Figure 3**a illustrates a film of AuNPs covered with two types of ligands: *n*-hexanethiols and alkanethiols terminated in oligo(ethylene glycols), EG_n, where n denotes the number of ethylene glycol units.[15a] These ligands are phase-separated and form disjoint domains (often referred to as "stripes" although it must be remembered that the regularity of the stipes has been a subject of a rather heated controversy[24]). In particular, the EG_n domains can tightly bind various cations with selectivity of this binding (against other, competing ions) depending on the number of EG units. When such cations bind, they effectively lower the height of the potential barrier between proximal NPs and thus facilitate electron transport (Figure 3b).[20a,25] In addition, it is not necessary to bind cations between every pair of nearby NPs to markedly increase the film's conductivity—in fact, forming only one (or few) conductive paths though the film suffices. Consequently, the films exhibit detectable changes in conductance when immersed in ultralow-concentration solutions of analytes—with EG_3 thiols, the film selectively detects highly poisonous methyl mercury down to attomolar levels (versus standard detection limits at already toxic $\approx 1 \times 10^{-9}$ M levels[26]); with EG_2 thiols, it selectively detects Cd^{2+} at $\approx 1 \times 10^{-12}$ M concentrations (Figure 3c).

Accurate sensing is also possible with mixed SAMs not forming phase-separated domains. For example, AuNPs stabilized with SAMs comprising *N*-acetyl-L-cysteine (which binds metal ions strongly) and protonated MUA thiols (which bind metal ions weakly but enhance binding selectivity) show appreciable selectivity toward Ag^+ and Pb^{2+} with 10^{-13} and 10^{-11} M detection limits, respectively (Figure 3d).[14] Additionally, we demonstrated humidity sensors based on TMA-stabilized AuNPs and gas sensors based on MUA-covered AuNPs nanoparticles.[14] In the former, increase in ambient humidity and in the concomitant water content in the film translates into reduced magnitude of electrostatic attractions between the positively charged particles and the surrounding Cl^- counterions—in effect, the counterions become more mobile and their capacitive migration changes film's apparent conductivity. When humidity increases from ≈0% to 100%, the apparent conductivity increases by a remarkable four orders of magnitude. The chemically modulated mobility of counterions is also operative in MUA-based gas sensors. When a layer of protonated MUA nanoparticles is exposed to flowing ammonia gas, the acid–base reaction produces mobile ammonium counterions. These ions give rise to ionic current, effectively decreasing the resistance by three to four orders of magnitude.

5. Chemoelectronic Logic Circuits

The last step of our effort has been integration of the individual elements into full circuits performing logical operations on various combinations of chemical inputs (**Figure 4**a).[14] Initially, we combined the bilayer diodes and resistors (the latter made of uncharged AuNPs) into the "AND" and "OR" logic gates. The circuit schemes are illustrated in the upper portion of Figure 4b while their experimental characteristics are shown in Figure 4c—for the "AND" gate, high output potential ("1") is recorded only when both "A" and "B" inputs are at high

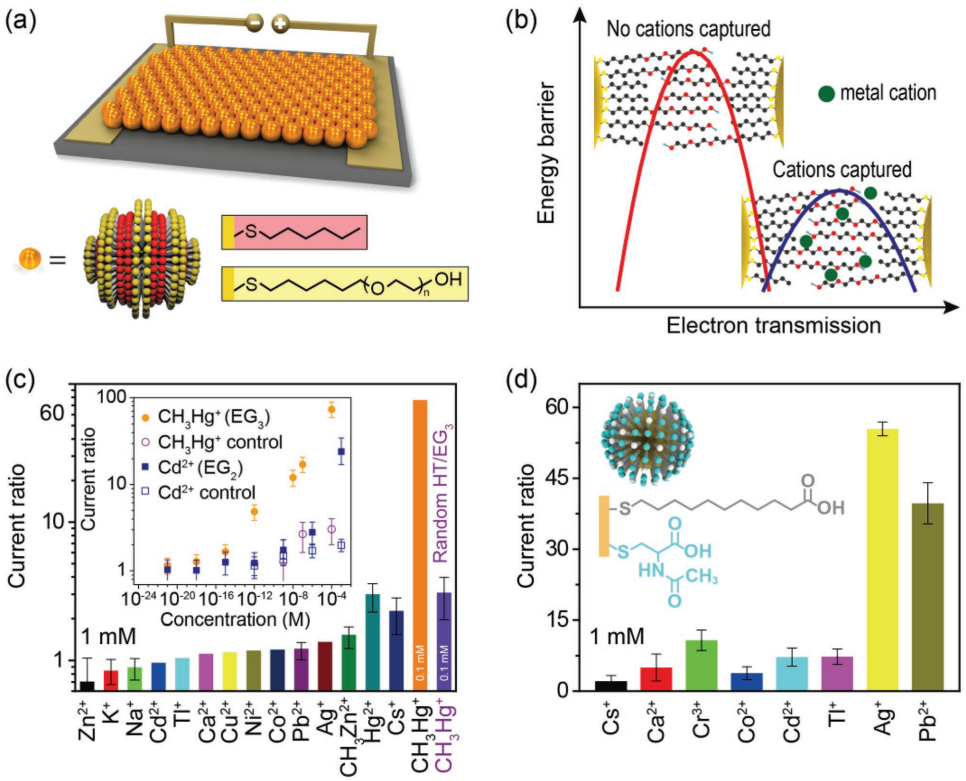

Figure 3. Films of metal nanoparticles in sensing applications. a) Scheme of a film of the so-called "striped" AuNPs used for ultrasensitive cation detection. b) Qualitative energy barriers between proximal NPs experienced by the tunneling electrons without (red) and with (blue) cations captured into the SAM. c) Selectivity of "striped" AuNPs decorated with HT/EG_3 SAMs towards different cations. Inset illustrates the sensitivity of AuNPs covered with HT/EG_3 SAM in detecting CH_3Hg^+ and of AuNPs covered with HT/EG_2 SAM in detecting Cd^{2+}. Current ratios are the ratios of currents recorded in the presence versus the absence of cations. Control devices correspond to nanoparticles covered with disordered/non-striped SAMs of the same composition. Error bars are calculated based on at least 12 independent devices. The sensitivity limits of the devices were determined by the two-sample *t*-test as the concentration of cations in solution at which the ratio of NP film's conductivity (current ratio) was greater than unity at the 99% confidence level. This confidence level corresponds to the *t*-statistic value smaller than "2.5" (or *p*-value larger than "0.01" and degree of freedom (*df*) larger than "22"). For detailed description see ref. [15a]. d) Selectivity of cation sensors based on AuNPs decorated with mixed SAMs of *N*-acetyl-L-cysteine and protonated MUA thiols. All metal cations are tested at a concentration of 1×10^{-3} M except for CH_3Hg^+ (0.1×10^{-3} M). a,c) Reproduced with permission.[15a] Copyright 2012, Springer Nature. d) Reproduced with permission.[14] Copyright 2016, Springer Nature.

potentials; for the "OR" gate, however, the output is "1" when either "A" or "B" inputs are at high potential. Subsequently, we combined the "OR" and "NOR" gates (lower portion of Figure 4b) with inputs from NP-based humidity and NH_3/HCl gas sensors (Figure 4d), humidity and silver cation sensors (Figure 4e), and lead and chromium cation sensors (Figure 4f). In these circuits, the input "0" and "1" states corresponded to, respectively, the low (≈0%) and high humidity (≈100%), exposure to HCl/NH_3 gas, or absence versus presence of cations. In the "OR" circuit, the output was at low potential only when both inputs were "0" (for example, ≈0% humidity and absence of Ag^+ in Figure 4e). In the "NOR" circuit, the output was at high potential only when both inputs were at "0" states (e.g., absence of both Pb^{2+} and Cr^{3+} cations in Figure 4f). The sensors gave these readings within ≈1 s from the exposure to signals and were reusable multiple times when washed with solutions of chelating agents (e.g., EDTANa).

While many other combinations and more inputs can be easily envisioned, one needs to consider whether such extensions would not entail manufacturing complications. In this regard, the ease with which the circuits are made needs to be emphasized—they are simply cast from ethanolic solutions and left to dry. While, so far, we have been "pipetting" the devices manually, we can easily envision ink-jet printing them at much higher speeds and much better spatial resolutions. Another aspect worth mentioning is that the devices are really hard to break mechanically—because of their granular nature, films deposited onto flexible substrates can be bent by ≈45° (Figure 4a inset, blue photograph) yet they still function properly and are quite resilient over many bending/unbending cycles. Last but not least, the circuits are completely nontoxic as the constituent gold AuNPs are not only benign but also beneficial, exhibiting antibacterial properties (for Gram-selective properties of charged AuNPs similar to those we use here, see ref. [27]).

6. Extensions and Outlook

The ideas outlined above are gradually getting traction in the community and new, often quite ingenious applications of modulated conductance though NP films emerge. For

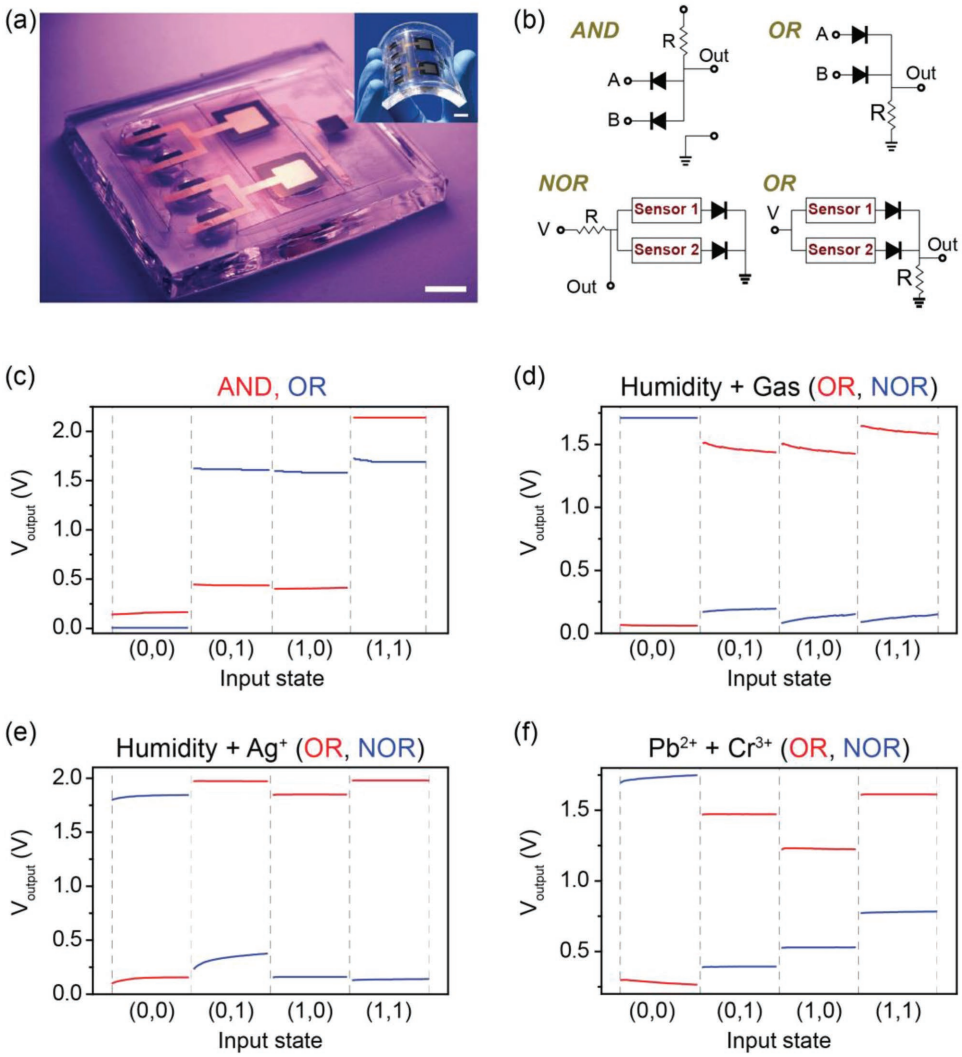

Figure 4. Logic gates and "chemoelectronic" circuits made of metal nanoparticles. a) A photograph of a typical circuit comprising two types of sensors (each in duplicate at the "arms" of the two golden "forks") and two diodes (square elements in the center). The diodes are fully embedded in PDMS; the sensors have their top surface open to the atmosphere. The inset is the photograph of device upon mechanical bending. Scale bar = 1 cm. b) Schemes and c–f) performance characteristics of the AND, OR, and NOR logic gates assembled from all-gold-nanoparticle components—diodes, sensors, and resistors. The devices comprised (c), diodes and resistors, (d–f), diodes, resistors and various pairs of NP sensors. In all gates, an input of "*0*"/"*1*" represents 0/2 volts, low/high humidity, HCl/NH_3 gas, and the absence/presence of the metal ions. Reproduced with permission.[14] Copyright 2016, Springer Nature.

example, Zhang et al.[28] used MUA-covered AuNPs to detect Hg^{2+} selectively (at 0.1×10^{-9} M levels), whereas Lin et al.[29] enhanced the conductivity changes by coupling NPs to the material's mechanical response. In Lin's system, AuNPs presenting aptamers having high affinity to specific macromolecular targets were attached to polymer chains. Binding of the targets in-between the NPs caused the shrinkage of the polymer matrix, in effect bringing the AuNPs closer together and increasing material's conductivity. In this way, the binding effect was amplified, and the sensors could detect thrombin at attomolar concentrations or low-molecular-weight anatoxin at the 10^{-14} M level, in both cases selectively and reproducibly. There has also been progress in understanding the physics underlying chemoelectronic systems. In an interesting study, Rotello and co-workers[30] used impedance spectroscopy to probe the behavior of AuNP films under periodic ac bias, and were able to distinguish the ionic and electronic charge-transport components for different particle-stabilizing ligands. Boon and de la Cruz performed simulations[31] based on the Nernst–Planck model to demonstrate the feasibility of a field-effect transistor based on immobile polyelectrolyte (akin to our immobile charged NPs) and mobile counterions. This theoretical work links with our ongoing experimental effort on progressing from chemoelectronic diodes to transistors, which has proven quite difficult. For bipolar junction transistor (n–p–n or p–n–p), the major problem has been the controlled deposition and wiring of a very thin middle-layer base. For field-effect transistors (FETs), we initially had to apply relatively large potentials (to achieve rapid response and sharp counterion gradients) which, unfortunately, damaged the NPs—we

solved this problem recently using porous high-capacitance carbon electrodes and the paper on the topic is forthcoming. The advantages of such electrodes are evident also in our most recent work[18] in which we made diodes using just one type of charged NPs (positively charged TMA AuNPs) but sandwiched between two different electrodes, Au and porous graphene/carbon nanotube composite (G/CNT). The role of the G/CNT electrode is to absorb the Cl^- counterions stripped under bias from the NPs. In this way, much steeper counterion gradients within AuNP layer can be achieved, translating into significantly improved rectification ratios (up to ≈50) and much shorter switching times (approximately tens of ms for currents to saturate and single ms to reach rectification ratios of ≈20, see ref. [18]), ultimately allowing the Au-NP-G/CNT laminates to transduce 500 kHz radio signals. We note that such switching times are already becoming commensurate with those of common polymer-based electronics,[16] though the rectification ratios are still lower. Also, whereas organic-electronics materials can be used for information storage (including multilevel memories[32]), our counterion gradients dissipate with time, erasing any spatially-encoded information. To be useful in memory elements, the counterion gradients would have to be "frozen" in time, which appears a difficult albeit not impossible proposition (e.g., by using organic counterions that could be photo-crosslinked such that their diffusion coefficient decreases markedly). Looking forward, we envision chemoelectronics adding a new angle to the effort on the so-called nanobioelectronics, to date largely based on nanotubes and graphene devices.[33] Because chemoelectronic circuits can function in humid/wet environments and the NPs can be easily functionalized with various types of ligands[34a]—including those that interact selectively with cells and those that can bind certain metabolites, chemokines, etc., these cells emit[34b]—the NP films could simultaneously serve as substrates for culture growth and as sensors monitoring, say, metabolic activity (with very low detection limits).

Overall, it is evident from our discussion that chemoelectronics is not intended to compete with orders-of-magnitude-faster semiconductor devices—the timescales for establishing ionic gradients, even at very small distances (e.g., across a one-NP-thick film), are simply not commensurate with those of electronic transitions in semiconductors. On the other hand, the ease of chemical functionalization of the NPs and the ability to tailor responses of the flexible NP films to desired analytes make this form of electronics appealing in chemical, mechanochemical, and biological sensing applications. As we continue our own work on improving the performance characteristics of these unusual nanostructured materials, we hope that after reading this article, the readers will find more interesting twists to the unveiling story of chemoelectronics.

Acknowledgements

X.Z., Y.Z., and Y.Y. acknowledge the support from the National Natural Science Foundation of China (21571039) and the Chinese Academy of Sciences. B.A.G. gratefully acknowledges generous support from the Institute for Basic Science Korea, Project Code IBS-R020-D1.

Conflict of Interest

The authors declare no conflict of interest.

Keywords

chemoelectronic circuits, ionic gradients, logic gates, metal nanoparticles, sensors

Received: July 28, 2018
Revised: November 8, 2018
Published online:

[1] S. M. Sze, K. K. Ng, *Physics of Semiconductor Devices*, John Wiley & Sons, Hoboken, NJ, USA **2007**.
[2] a) A. P. Alivisatos, *Science* **1996**, *271*, 933; b) D. V. Talapin, J.-S. Lee, M. V. Kovalenko, E. V. Shevchenko, *Chem. Rev.* **2010**, *110*, 389.
[3] a) H. Sirringhaus, T. Kawase, R. H. Friend, T. Shimoda, M. Inbasekaran, W. Wu, E. P. Woo, *Science* **2000**, *290*, 2123; b) C. Wang, H. Dong, W. Hu, Y. Liu, D. Zhu, *Chem. Rev.* **2012**, *112*, 2208; c) G.-J. N. Wang, A. Gasperini, Z. Bao, *Adv. Electron. Mater.* **2018**, *4*, 1700429.
[4] a) F. Schwierz, *Nat. Nanotechnol.* **2010**, *5*, 487; b) M. M. Shulaker, G. Hills, N. Patil, H. Wei, H.-Y. Chen, H. S. PhilipWong, S. Mitra, *Nature* **2013**, *501*, 526; c) C. Qiu, Z. Zhang, M. Xiao, Y. Yang, D. Zhong, L.-M. Peng, *Science* **2017**, *355*, 271.
[5] a) Q. Liu, L. Yu, H. Li, R. Qin, Z. Jing, J. Zheng, Z. Gao, J. Lu, *J. Phys. Chem. C* **2011**, *115*, 6933; b) K. S. Novoselov, A. K. Geim, S. V. Morozov, D. Jiang, Y. Zhang, S. V. Dubonos, I. V. Grigorieva, A. A. Firsov, *Science* **2004**, *306*, 666.
[6] a) C. B. Murray, C. R. Kagan, M. G. Bawendi, *Annu. Rev. Mater. Sci.* **2000**, *30*, 545; b) K. L. Kelly, E. Coronado, L. L. Zhao, G. C. Schatz, *J. Phys. Chem. B* **2003**, *107*, 668.
[7] a) C. Farcau, N. M. Sangeetha, H. Moreira, B. Viallet, J. Grisolia, D. Ciuculescu-Pradines, L. Ressier, *ACS Nano* **2011**, *5*, 7137; b) P. Zhang, H. Bousack, Y. Dai, A. Offenhaeusser, D. Mayer, *Nanoscale* **2018**, *10*, 992; c) N. Decorde, N. M. Sangeetha, B. Viallet, G. Viau, J. Grisolia, A. Coati, A. Vlad, Y. Garreau, L. Ressier, *Nanoscale* **2014**, *6*, 15107.
[8] a) M. A. Mangold, M. Calame, M. Mayor, A. W. Holleitner, *J. Am. Chem. Soc.* **2011**, *133*, 12185; b) M. A. Mangold, M. Calame, M. Mayor, A. W. Holleitner, *ACS Nano* **2012**, *6*, 4181.
[9] a) B. Teschome, S. Facsko, T. Schoenherr, J. Kerbusch, A. Keller, A. Erbe, *Langmuir* **2016**, *32*, 10159; b) H. Joh, S.-W. Lee, M. Seong, W. S. Lee, S. J. Oh, *Small* **2017**, *13*, 1700247.
[10] K. Saha, S. S. Agasti, C. Kim, X. Li, V. M. Rotello, *Chem. Rev.* **2012**, *112*, 2739.
[11] a) S. Willing, H. Lehmann, M. Volkmann, C. Klinke, *Sci. Adv.* **2017**, *3*, e1603191; b) O. Bitton, D. B. Gutman, R. Berkovits, A. Frydman, *Nat. Commun.* **2017**, *8*, 402; c) K. S. Makarenko, Z. Liu, M. P. de Jong, F. A. Zwanenburg, J. Huskens, W. G. van der Wiel, *Adv. Mater.* **2017**, *29*, 1702920.
[12] a) A. M. Kalsin, B. Kowalczyk, S. K. Smoukov, R. Klajn, B. A. Grzybowski, *J. Am. Chem. Soc.* **2006**, *128*, 15046; b) A. O. Pinchuk, A. M. Kalsin, B. Kowalczyk, G. C. Schatz, B. A. Grzybowski, *J. Phys. Chem. C* **2007**, *111*, 11816.
[13] H. Nakanishi, D. A. Walker, K. J. M. Bishop, P. J. Wesson, Y. Yan, S. Soh, S. Swaminathan, B. A. Grzybowski, *Nat. Nanotechnol.* **2011**, *6*, 740.
[14] Y. Yan, S. C. Warren, P. Fuller, B. A. Grzybowski, *Nat. Nanotechnol.* **2016**, *11*, 603.
[15] a) E. S. Cho, J. Kim, B. Tejerina, T. M. Hermans, H. Jiang, H. Nakanishi, M. Yu, A. Z. Patashinski, S. C. Glotzer, F. Stellacci,

B. A. Grzybowski, *Nat. Mater.* **2012**, *11*, 978; b) H. Nakanishi, K. J. M. Bishop, B. Kowalczyk, A. Nitzan, E. A. Weiss, K. V. Tretiakov, M. M. Apodaca, R. Klajn, J. F. Stoddart, B. A. Grzybowski, *Nature* **2009**, *460*, 371.

[16] a) D. A. Bernards, S. Flores-Torres, H. D. Abruna, G. G. Malliaras, *Science* **2006**, *313*, 1416; b) C. V. Hoven, H. Wang, M. Elbing, L. Garner, D. Winkelhaus, G. C. Bazan, *Nat. Mater.* **2010**, *9*, 249.

[17] N. R. Jana, X. Peng, *J. Am. Chem. Soc.* **2003**, *125*, 14280.

[18] X. Zhao, B. Tu, M. Li, X. Feng, Y. Zhang, Q. Fang, T. Li, B. A. Grzybowski, Y. Yan, *Sci. Adv.* **2018**, *4*, eaau3546.

[19] a) W. P. Wuelfing, S. J. Green, J. J. Pietron, D. E. Cliffel, R. W. Murray, *J. Am. Chem. Soc.* **2000**, *122*, 11465; b) R. H. Terrill, T. A. Postlethwaite, C. H. Chen, C. D. Poon, A. Terzis, A. D. Chen, J. E. Hutchison, M. R. Clark, G. Wignall, J. D. Londono, R. Superfine, M. Falvo, C. S. Johnson, E. T. Samulski, R. W. Murray, *J. Am. Chem. Soc.* **1995**, *117*, 12537.

[20] a) A. Zabet-Khosousi, A.-A. Dhirani, *Chem. Rev.* **2008**, *108*, 4072; b) G. R. Wang, L. Wang, R. Qiang, J. Wang, J. Luo, C.-J. Zhong, *J. Mater. Chem.* **2007**, *17*, 457.

[21] E. Boubour, R. B. Lennox, *J. Phys. Chem. B* **2000**, *104*, 9004.

[22] a) L. M. H. Lai, I. Y. Goon, K. Chuah, M. Lim, F. Braet, R. Amal, J. J. Gooding, *Angew. Chem. Int. Ed.* **2012**, *51*, 6456; b) L. Shao, J. J. Diao, Z. Tang, S. Liu, S. C. Shen, J. Liu, X. Rui, D. Yu, Q. Zhao, *Nanoscale* **2014**, *6*, 4089; c) Z. Guo, Z.-G. Liu, X.-Z. Yao, K.-S. Zhang, X. Chen, J.-H. Liu, X.-J. Huang, *Sci. Rep.* **2013**, *3*, 3115; d) Y. Zhang, J. Liu, D. Li, X. Dai, F. Yan, X. A. Conlan, R. Zhou, C. J. Barrow, J. He, X. Wang, W. Yang, *ACS Nano* **2016**, *10*, 5096; e) B. Raguse, E. Chow, C. S. Barton, L. Wieczorek, *Anal. Chem.* **2007**, *79*, 7333.

[23] a) H. Wohltjen, A. W. Snow, *Anal. Chem.* **1998**, *70*, 2856; b) L. Han, D. R. Daniel, M. M. Maye, C.-J. Zhong, *Anal. Chem.* **2001**, *73*, 4441; c) F. J. Ibanez, U. Gowrishetty, M. M. Crain, K. M. Walsh, F. P. Zamborini, *Anal. Chem.* **2006**, *78*, 753; d) X. Shi, N. N. Kariuki, M. Schadt, G. R. Wang, Q. Rendeng, J. Choi, J. Luo, S. Lu, C.-J. Zhong, *J. Am. Chem. Soc.* **2007**, *129*, 2161; e) W. H. Steinecker, M. P. Rowe, E. T. Zellers, *Anal. Chem.* **2007**, *79*, 4977; f) R. A. Potyrailo, *Chem. Soc. Rev.* **2017**, *46*, 5311; g) F. J. Ibanez, F. P. Zamborini, *Small* **2012**, *8*, 174.

[24] a) A. M. Jackson, J. W. Myerson, F. Stellacci, *Nat. Mater.* **2004**, *3*, 330; b) G. A. DeVries, M. Brunnbauer, Y. Hu, A. M. Jackson, B. Long, B. T. Neltner, O. Uzun, B. H. Wunsch, F. Stellacci, *Science* **2007**, *315*, 358.

[25] R. E. Holmlin, R. Haag, M. L. Chabinyc, R. F. Ismagilov, A. E. Cohen, A. Terfort, M. A. Rampi, G. M. Whitesides, *J. Am. Chem. Soc.* **2001**, *123*, 5075.

[26] a) P. Namour, M. Lepot, N. Jaffrezic-Renault, *Sensors* **2010**, *10*, 7947; b) A. Ivask, K. Hakkila, M. Virta, *Anal. Chem.* **2001**, *73*, 5168; c) A. Rantala, M. Utriainen, N. Kaushik, M. Virta, A.-L. Vaelimaa, M. Karp, *Anal. Bioanal. Chem.* **2011**, *400*, 1041; d) E. Climent, M. Dolores Marcos, R. Martinez-Manez, F. Sancenon, J. Soto, K. Rurack, P. Amoros, *Angew. Chem., Int. Ed.* **2009**, *48*, 8519.

[27] P. P. Pillai, B. Kowalczyk, K. Kandere-Grzybowska, M. Borkowska, B. A. Grzybowski, *Angew. Chem., Int. Ed.* **2016**, *55*, 8610.

[28] P. Zhang, Z. Lyu, J. Viktorova, A. Offenhaeusser, L. Feng, D. Mayer, *Biosens. Bioelectron.* **2018**, *117*, 450.

[29] Z.-T. Lin, J. Gu, C.-H. Li, T. R. Lee, L. Xie, S. Chen, P.-Y. Cao, S. Jiang, Y. Yuan, X. Hong, H. Wang, D. Wang, X. Wang, G.-B. Jiang, M. Heon, T. Wu, *Adv. Mater.* **2017**, *29*, 1702090.

[30] X. Yu, N. Malvankar, R. Landis, S. Eymur, O. R. Miranda, V. M. Rotello, *Small* **2015**, *11*, 3814.

[31] N. Boon, M. O. de la Cruz, *Soft Matter* **2015**, *11*, 4793.

[32] G. de Ruiter, Y. H. Wijsboom, N. Oded, M. E. van der Boom, *ACS Appl. Mater. Interfaces* **2010**, *2*, 3578.

[33] a) A. Noy, *Adv. Mater.* **2011**, *23*, 807; b) A. Zhang, C. M. Lieber, *Chem. Rev.* **2016**, *116*, 215.

[34] a) D. Witt, R. Klajn, P. Barski, B. A. Grzybowski, *Curr. Org. Chem.* **2004**, *8*, 1763; b) T. Sun, D. Han, K. Rhemann, L. Chi, H. Fuchs, *J. Am. Chem. Soc.* **2007**, *129*, 1496.